ACS Partner Journal

CHEMICAL & BIOMEDICAL IMAGING

Open Access

pubs.acs.org/ChemBioImaging

Article

Line-Shifting Triarylmethyl Radicals for Imaging of Enzyme Activity Using Overhauser-Enhanced Magnetic Resonance Imaging: Application to Alkaline Phosphatase

Murugesan Velayutham, Martin Poncelet, Ayano Enomoto, Justin L. Huffman, Virat G. Pandya, Kazuhiro Ichikawa, Valery V. Khramtsov, and Benoit Driesschaert*

Cite This: *Chem. Biomed. Imaging* 2025, 3, 35−44

Read Online

ACCESS | Metrics & More | Article Recommendations | Supporting Information

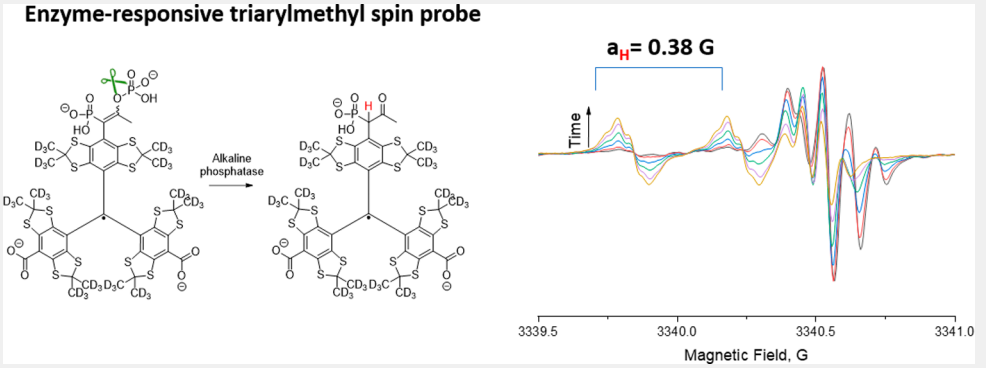

ABSTRACT: Enzyme catalytic activities are critical biomarkers of tissue states under physiological and pathophysiological conditions. However, the direct measurement and imaging of enzyme activity *in vivo* remains extremely challenging. We report the synthesis and characterization of the first stable triarylmethyl (TAM) radical substrate of alkaline phosphatase (TAM-ALPs). The enzymatic dephosphorylation of TAM-ALPs results in a drastic change in its electron paramagnetic resonance (EPR) spectrum that can be used to image enzyme activity using EPR-based technologies. TAM-ALPs and their enzyme products were fully characterized using EPR and HPLC-MS techniques. A proof of concept of imaging enzyme activity using Overhauser-enhanced magnetic resonance imaging was demonstrated *in vitro*. This study clearly demonstrates the potential of EPR-based imaging technologies associated with TAM spin probes to map enzyme activity *in vivo* in future studies.

KEYWORDS: *EPR, TAM radical, enzyme activity, alkaline phosphatase, OMRI*

INTRODUCTION

Enzymes play a critical role in the physiology and physiopathology of living organisms. Enzyme activities are important clinical biomarkers used to diagnose and monitor disease status/conditions. While many chemical and biochemical methods are available to measure enzyme activity *in vitro* and *ex vivo*, the assessment of the activity of an enzyme directly within its natural environment *in vivo,* while arguably more relevant, remains very challenging today.[1] For *in vivo* imaging of enzyme activity, magnetic resonance-based modalities such as magnetic resonance imaging (MRI), low-frequency electron paramagnetic resonance imaging (EPRI, also named electron MRI, e-MRI), or a hybrid modality such as Overhauser-enhanced MRI (OMRI) have the advantage of high penetration depth.[2−5] Indeed, optical techniques suffer from light absorption and scattering within the tissues. Recently, the concept of line-shifting nitroxide has been proposed to assess enzyme activity using EPR-based technologies.[6−8] Those are TEMPONE-based nitroxide radicals that are substrates of a particular enzyme. The enzymatic conversion of substrates to products is associated with a shift in the product EPR lines due to a change in molecular structure. The kinetics of the spectral conversion can be used to assess the enzyme activity (Figure 1A). While these nitroxides were initially designed to image enzyme activity by OMRI, we recently demonstrated their application to image enzyme activity using EPR with a nitroxide substrate of alkaline phosphatase.[9] However, the fast bioreduction of TEMPONE-based nitroxides to EPR silent hydroxylamines prevents their application *in vivo*.[10] On the other hand, water-soluble

Received: August 6, 2024
Revised: November 12, 2024
Accepted: November 15, 2024
Published: November 23, 2024

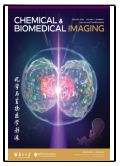

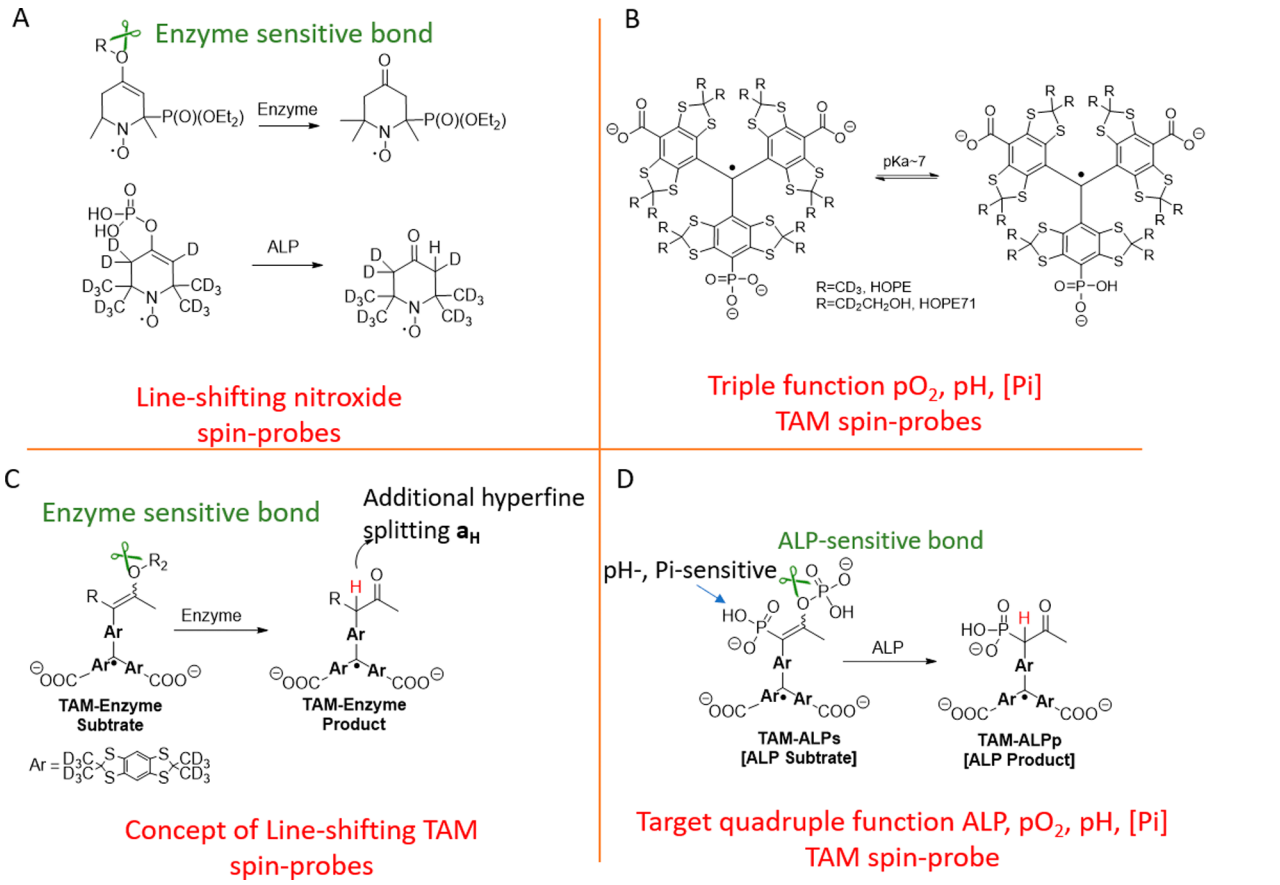

Figure 1. (A) Line-shifting nitroxide radicals. (B) Triple function TAM radicals. (C) Concept of line-shifting TAM radicals. (D) Target quadruple function ALP, pO_2, pH, [Pi] TAM radical. ALP: alkaline phosphatase, pO_2: partial pressure of oxygen, [Pi]: concentration of inorganic phosphate.

triarylmethyl (TAM) radicals (Figure 1B) show unprecedented stability in biological media[11,12] and have been used *in vivo* to map tissue oxygen for decades.[13,14] However, their synthesis, chemical modifications, and commercial availability remain more challenging.

While TAMs EPR spectra have an intrinsic spectral sensitivity to pO_2 through Heisenberg spin exchange, para-phosphonate TAM radicals such as HOPE[15,16] or HOPE71[17] (Figure 1B) have been recently developed as triple function pO_2, pH, and inorganic phosphate (Pi) concentration spin probes. Those radicals are used routinely to assess and map those important parameters *in vivo* with application in cancer research.[17−20]

Here we report the first prototype of line-shifting TAM radicals to enable *in vivo* measurement of enzyme activity using EPR-based imaging technology. The mechanism of sensitivity to enzyme activity is based on the appearance of a hydrogen hyperfine splitting upon enzymatic cleavage of an enzyme-sensitive bond followed by a keto−enol tautomerization (Figure 1C), like line-shifting nitroxides. To provide additional pH and Pi sensitivity, a phosphonic acid was included in the design (Figure 1D). In this article, we report on the progress toward the development of quadruple function alkaline phosphatase (ALP), pO_2, pH, and [Pi] TAM spin probes. ALP is an important biological enzyme in living organisms that catalyzes the hydrolysis of phosphate groups from nucleic acids, proteins, and other substrates. ALP is widely present in various human tissues such as bone, liver, kidney, intestine, and placenta.[21] Under physiological conditions, the normal ALP activity concentration in human serum ranges between 46−190 mU/mL.[22] However, the ALP activity in the serum increases under various pathophysiological conditions.[21] Hence, ALP is considered a potential biomarker of many disorders/diseases.[23−26] Therefore, the sensitive, rapid, and simple determination of ALP activity in the serum and tissues is of great significance for the clinical diagnosis of ALP-related diseases.

RESULTS AND DISCUSSION

Synthesis of TAM-ALPs

The target ALP substrate TAM-ALPs were successfully synthesized in four steps from the known intermediate **1**,[27] as depicted in Scheme 1. First, the triarylmethyl cation was generated upon treatment of **1** with triflic acid. The addition of dimethyl acetonylphosphonate anion to the triaryl carbonium resulted in an *ipso*-aromatic substitution of the para-hydrogen, leading to the radical **2**. This ipso-nucleophilic substitution of TAM cation leading to a TAM radical has been reported previously.[28−30] Then, the enolate, generated by the treatment of **2** with lithium diisopropyl amide (LDA) was reacted with dimethyl chlorophosphate, leading to the protected enol-phosphate **3**. Finally, the phosphonic acids and phosphate moieties were deprotected with TMSBr while the esters were hydrolyzed using LiOH to provide TAM-ALPs. The purity of TAM-ALPs was determined to be >95% by HPLC.

https://doi.org/10.1021/cbmi.4c00059
Chem. Biomed. Imaging 2025, 3, 35−44

Scheme 1. Synthesis of TAM-ALPs

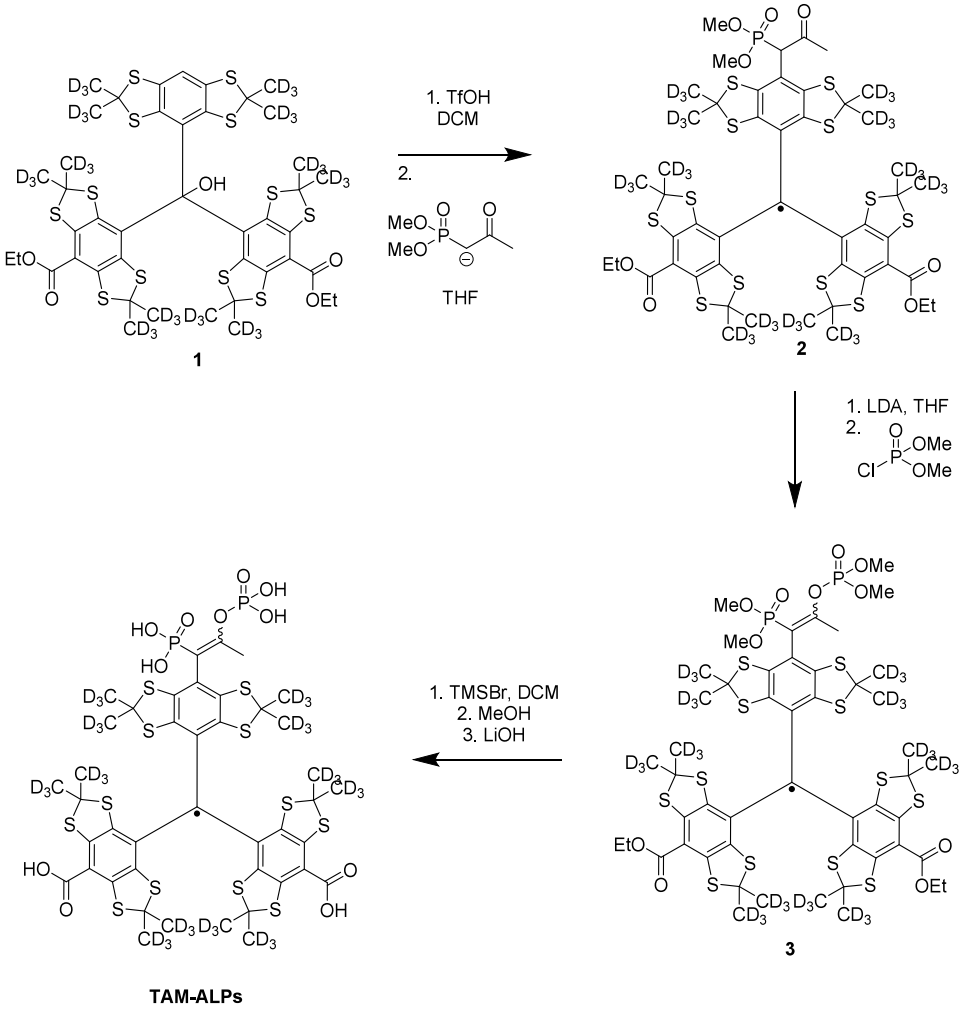

EPR Characterization of TAM-ALPs

TAM-ALPs was characterized using X-band EPR spectroscopy. The EPR spectrum of 0.2 mM TAM-ALPs in Tris buffer, recorded under room air conditions, exhibits a doublet pattern due to the interaction of the unpaired electron with the ^{31}P (hyperfine coupling) of the phosphonic acid group (Figure 2 and SI Figure S6). Interestingly, the measured hyperfine splitting constant (hfs) of 5.71 G is almost twice as large as for the HOPE probe,[16] in which the phosphorus nucleus is located one bond closer to the radical center. Upon deoxygenation of the solution, the narrowing of the lines reveals additional smaller hyperfine splittings. The additional apparent quintet with an hfs ~100 mG was assigned to additional hyperfine splittings with the three equivalents ^{1}H of the methyl group and the ^{31}P of the phosphate group with similar hfs (Figure 2B). The spectrum simulated using the isotropic hyperfine splitting values of $a_{P\alpha}$ = 5.71 G, $a_{P\beta}$ = 0.11 G, and a_H = 0.09 G is in excellent agreement with the experimental spectrum. It is worth mentioning that the vinyl phosphate moiety can exist in either *E* or *Z* configurations. However, EPR and HPLC analyses demonstrated the presence of only one of these two stereoisomers. The exact configuration of the alkene was not determined.

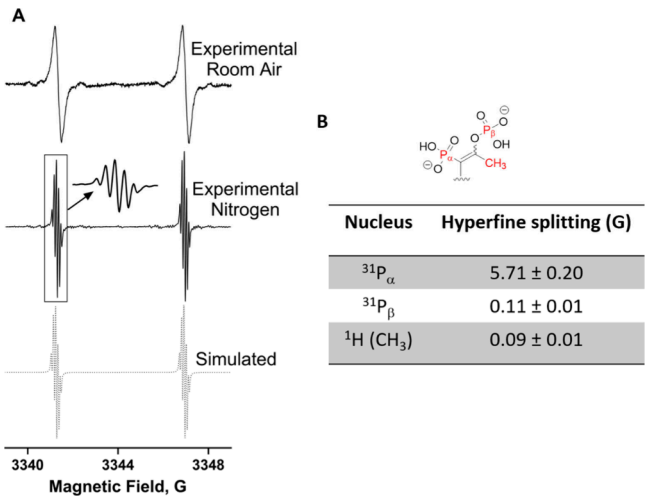

Figure 2. (A) X-band EPR spectra of 0.2 mM TAM-ALPs radical in 10 mM Tris buffer (pH = 7.5) containing NaCl (0.9%), $MgCl_2$ (1 mM), and $ZnCl_2$ (0.1 mM) under room air (top) and nitrogen (middle) at 37 °C and simulated spectrum. (B) Hyperfine splitting values.

Next, the sensitivity of TAM-ALPs to oxygen and pH was assessed. The spectra of 0.2 mM TAM-ALPs radical in 10 mM Tris buffer were recorded under various pO_2, and the oxygen-sensitive Lorentz peak-to-peak line width was plotted against pO_2. Figure 3A shows TAM-ALPs sensitivity of 0.51 ± 0.02 mG/mmHg in good agreement with oxygen sensitivity

https://doi.org/10.1021/cbmi.4c00059
Chem. Biomed. Imaging 2025, 3, 35−44

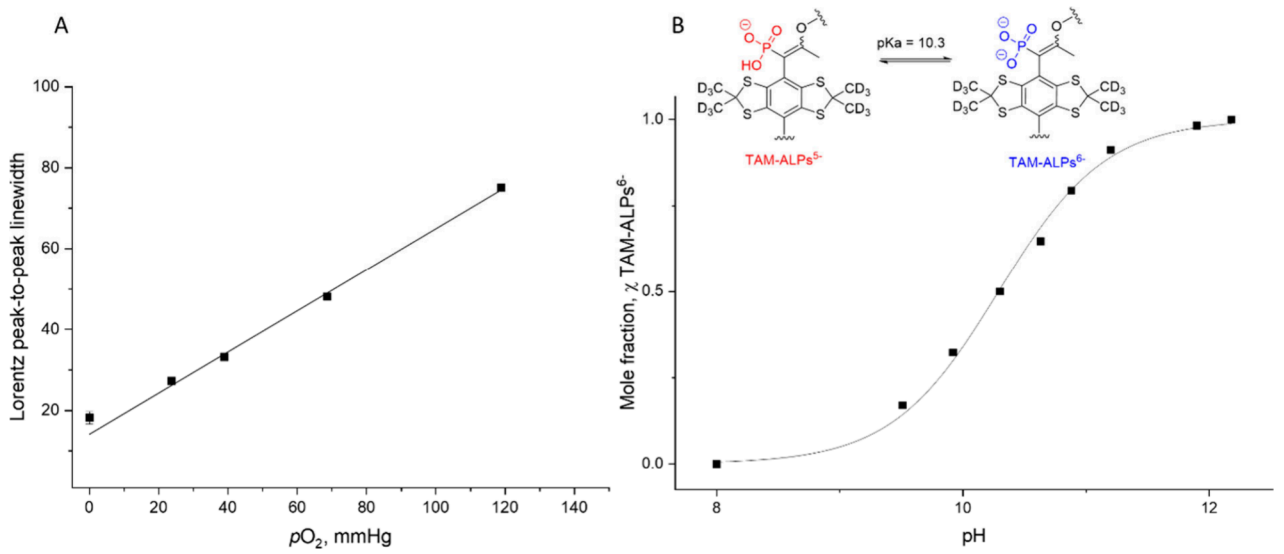

Figure 3. Sensitivity of TAM-ALPs to oxygen and pH. (A) Lorentz peak-to-peak line width versus pO_2, spectra were simulated with a Voigt function using 29 mG Gaussian peak-to-peak line width. The Lorentz line width shows a sensitivity to pO_2 of 0.51 ± 0.02 mG per mm Hg. TAM-ALPs 0.2 mM was dissolved in 10 mM Tris buffer containing 1 mM $MgCl_2$, 0.1 mM $ZnCl_2$, and 0.9% NaCl, pH 7.5 at 37 °C. (B) pH titration to determine pK_a. TAM-ALPs 0.3 mM was dissolved in 1 mM Tris buffer containing 1 mM $MgCl_2$, 0.1 mM $ZnCl_2$, and 0.9% NaCl and titrated with small amounts of NaOH or HCl at 37 °C (less than 1% dilution). The pK_a was determined to be 10.3 ± 0.1.

reported for similar triarylmethyl radicals.[31] To determine the pH sensitivity range, spectra of TAM-ALPs were recorded at various pH values from 7 to 13. For pH values close to the pK_a, the EPR spectra clearly show the presence of the two ionic species (see SI, Figure S2), namely TAM-ALPs^{5-} and TAM-ALPs^{6-} (Figure 3B). By plotting the mole fraction against the solution pH, a pK_a of 10.3 ± 0.1 was determined. Typically, pH can be measured for pH = pK_a ± 1.5 to ensure the presence of either ionic species in the spectrum. Therefore, TAM-ALPs could be used as a pH probe for a range of pH values from 8.8 to 11.8. While this range is too high to enable the measurement of pH in tissues, it could be interesting for *in vitro* applications to correlate alkaline phosphatase activity with pH in this particular range, as ALP has a maximum activity at pH = 8−10, depending on the conditions. Note that the phosphonate group has two pKs. However, for pH < 5, aggregation of the probe was observed because of the decreased aqueous solubility of the probe in its acid form when the phosphonate, phosphate, and carboxylic moieties become neutral/protonated. Of note, the phosphate group ionization was not visible on the EPR spectra because of the >50-fold lower hyperfine splitting between the phosphorus of the phosphate (P_α) than the phosphonate (P_β) groups.

EPR Studies of TAM-ALPs in the Presence of Alkaline Phosphatase Enzyme

With the sensitivity of TAM-ALPs to oxygen and pH determined, we then turned our attention to test the concept of line-shifting TAM. TAM-ALPs, 0.2 mM, was mixed with 1.2 U/mL of alkaline phosphatase (P6774−2KU, alkaline phosphatase from bovine intestinal mucosa, Sigma-Aldrich, USA), and the EPR time course was recorded (Figure 4 and SI Figures S7 and S8). Gratifyingly, the addition of ALP resulted in a change in EPR lines, validating that TAM-ALPs is a substrate of ALP and that the dephosphorylation results in visible changes in the EPR spectrum. A new spectral component labeled "#" progressively appears over time. This spectrum exhibits a new hyperfine splitting assigned to the

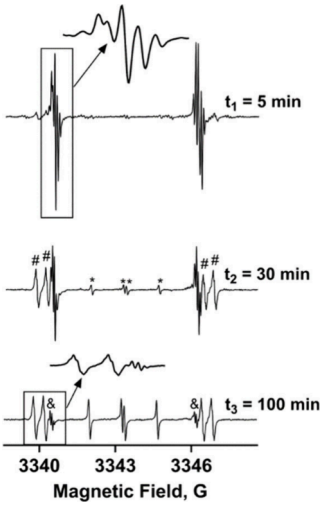

Figure 4. X-band EPR spectra of 0.2 mM TAM-ALPs with 1.2 U/mL of alkaline phosphatase in 10 mM Tris buffer containing 1 mM $MgCl_2$, 0.1 mM $ZnCl_2$, and 0.9% NaCl, pH 7.5 after 5, 30, and 100 min. EPR spectra were recorded at 37 °C. The sample in the cavity was flushed with nitrogen gas to maintain the sample under anoxic conditions during the EPR time course.

expected benzylic hydrogen and a larger phosphorus hfs. This spectrum is assigned to the expected dephosphorylated acetyl phosphonate TAM-ALP product. However, an additional doublet of doublet component, labeled "*", appeared unexpectedly soon after. The measured hfs of 1.4 and 1.3 G are consistent with the values found in benzylic methylene (CH_2) groups of TAM derivatives reported previously.[32,33] This observation suggests a second dephosphorylation independent of the enzyme. Hydrolysis of acetyl phosphonate in aqueous media has been reported in the literature and is known to depend on the particular structure.[34] In addition, a careful analysis of the spectra reveals a progressive conversion of the quintet pattern of the TAM-ALPs to a quartet labeled

https://doi.org/10.1021/cbmi.4c00059
Chem. Biomed. Imaging 2025, 3, 35−44

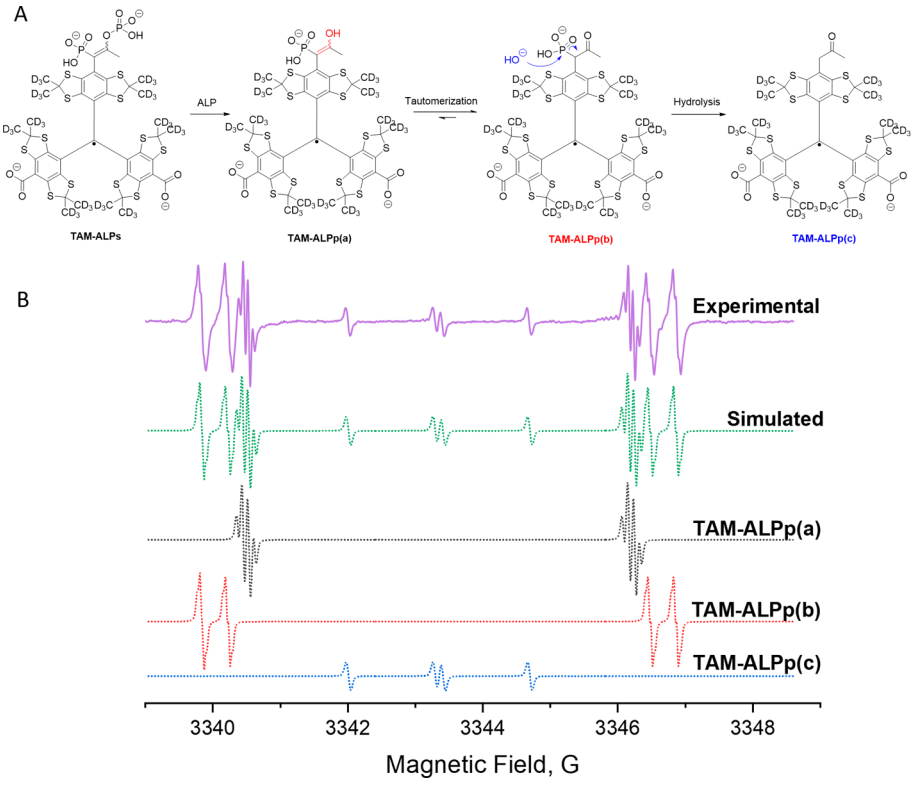

Figure 5. (A) ALP-triggered chain of reactions leading to TAM-ALPp(c) as the final product. (B) Experimental spectrum (solid line) obtained using the condition as in Figure 4 for time = 35 min was simulated (dotted line) using the following hyperfine coupling constants: for TAM-ALPp(a) a_P = 5.74 G, a_H = 0.09 G (3H); for TAM-ALPp(b) a_P = 6.68 G, a_H = 0.38 G, a_H = 0.04 G (3H); for TAM-ALPp(c) a_H = 1.41 G, a_H = 1.29 G. The deconvoluted simulated spectra of TAM-ALPp(a), TAM-ALPp(b), and TAM-ALPp(c) are also shown.

"&" in the spectra in Figure 4. This conversion is attributed to the enol form after dephosphorylation by the ALP.

The above observations allow us to formulate the following ALP-triggered reaction chain shown in Figure 5A. First, the ALP cleaves the phosphate group, leading to the enol form TAM-ALPp(a), which has a half-life sufficiently long to be observed on the EPR spectrum. Then, TAM-ALPp(a) undergoes a keto−enol tautomerization, leading to the expected TAM-ALPp(b). However, this derivative undergoes further hydrolysis of the phosphonate, leading to TAM-ALPp(c). Fitting the experimental spectra when all the species are present allows for the deconvolution of each spectral component presented in Figure 5B.

To further prove the identity of the three ALP-catalyzed products, the reaction was monitored using the HPLC-MS (Figure 6). Upon addition of ALP, the substrate peak (RT = 3.1 min, 1207 m/z) is converted to three new peaks having the same m/z (RT = 3.5 min, 1128 m/z, RT = 3.6 min, 1128 m/z, RT = 3.8 min, 1128 m/z). Those three peaks are attributed to the enol (one peak) and keto (two peaks) forms of TAM-ALPp(a-b). Indeed, TAM-ALPp(b) has a chiral carbon in addition to the atropisomerism (right- and left-handed enantiomeric propeller conformations) of the TAM itself.[35] This leads to two diastereoisomers for the case of TAM-ALPp(b) and two close peaks in HPLC. The chiral properties of TAM spin probes and resolution by HPLC have been reported previously.[36−38] Then, a peak (RT = 4.7 min, 1047 m/z) progressively increases, consistent with the formation of TAM-ALPp(c). Moreover, HPLC-MS study revealed the formation of an additional product (RT = 4.9 min, 2094 m/z, RT = 5.1 min, 2094 m/z, diastereoisomers) not seen on the

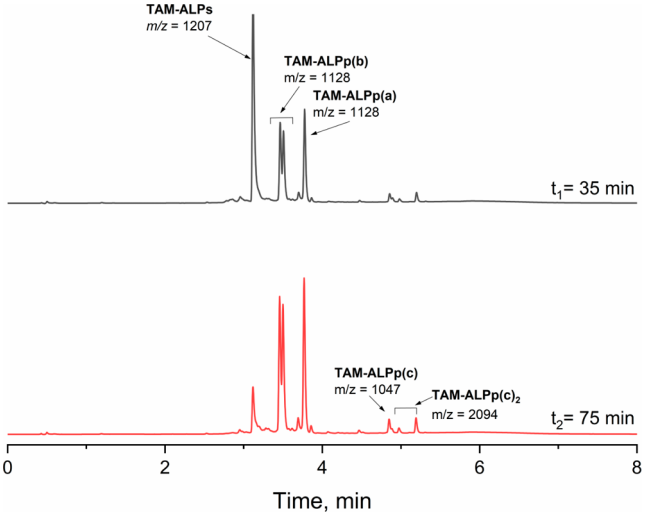

Figure 6. HPLC-MS chromatogram of 0.2 mM TAM-ALPs with 1.2 U/mL of alkaline phosphatase at 37 °C in 10 mM Tris buffer containing 1 mM $MgCl_2$, 0.1 mM $ZnCl_2$, and 0.9% NaCl, pH 7.5 after 35 and 75 min (see SI Figure S3 for MS spectra).

EPR spectra with a mass consistent with a dimer of TAM-ALPp(c) (see SI Figure S3 for MS spectra and molecular structures). Because of the biradical nature of this species, its EPR spectrum is expected to have a broad line width and, therefore, not visible under the parameters used to follow the enzymatic conversion of TAM-ALPs. Note that the keno-enol TAM-ALPp(b-a) could exist in equilibrium depending on the conditions. The spectrum of the reaction of TAM-ALPs with

https://doi.org/10.1021/cbmi.4c00059
Chem. Biomed. Imaging 2025, 3, 35−44

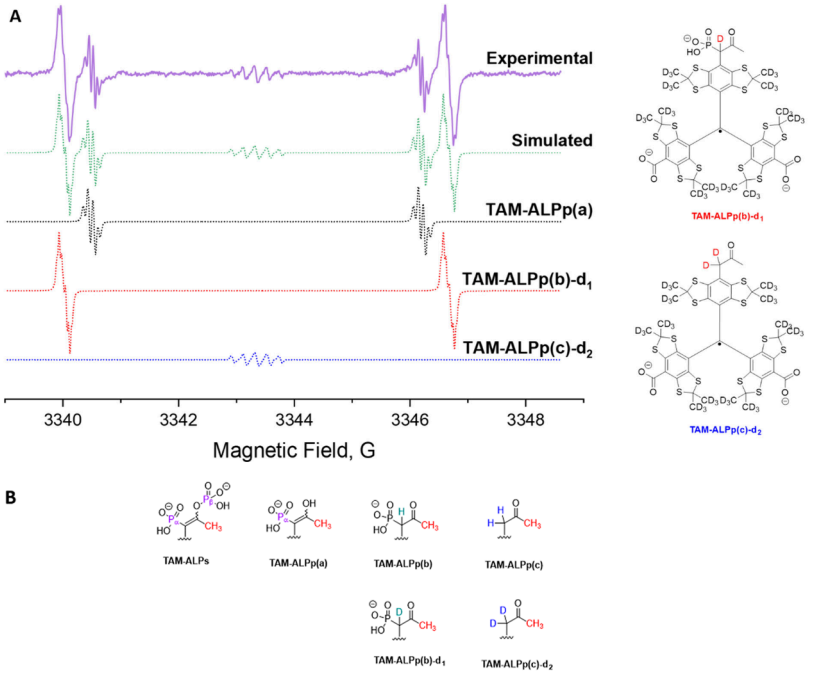

Hyperfine splitting constants (G)					
	$^{31}P_{\alpha}$	$^{31}P_{\beta}$	^{1}H (CH_3)	$^{1,2}H$ (CH)	$^{1,2}H$ (CH_2)
TAM-ALPs	5.71 ± 0.20	0.11 ± 0.01	0.09 ± 0.01	N.A.	N.A.
TAM-ALPp(a)	5.74 ± 0.20	N.A.	0.09 ± 0.01	N.A.	N.A.
TAM-ALPp(b)	6.68 ± 0.20	N.A.	0.04 ± 0.01	0.38 ± 0.04 (^{1}H)	N.A.
TAM-ALPp(b)-d_1	6.68 ± 0.20	N.A.	0.04 ± 0.01	0.06 ± 0.01 (^{2}H)	N.A.
TAM-ALP(c)	N.A.	N.A.	Unresolved	N.A.	1.41 ± 0.1 (^{1}H) 1.29 ± 0.1 (^{1}H)
TAM-ALP(c)-d_2	N.A.	N.A.	Unresolved	N.A.	0.22 ± 0.02 (^{2}H) 0.19 ± 0.02 (^{2}H)

Figure 7. (A) X-band EPR spectra of 0.2 mM TAM-ALPs and 1.2 U/mL of alkaline phosphatase in 10 mM Tris buffer in D_2O containing 1 mM $MgCl_2$, 0.1 mM $ZnCl_2$, and 0.9% NaCl, pH 7.5. EPR spectra were recorded 100 min after mixing the reactants at 37 °C. The sample in the cavity was flushed with nitrogen gas to obtain anoxic conditions. The experimental spectrum (solid line) was simulated (dotted line) using the following hyperfine splitting constants: TAM-ALPp(a) a_P = 5.74 G, a_H = 0.09 G (3H); for TAM-ALPp(b)-d_1 a_P = 6.68 G, a_D = 0.06 G, a_H = 0.04 G (3H); for TAM-ALPp(c)-d_2 a_D = 0.22 G, a_D = 0.19 G. The deconvoluted simulated spectra of TAM-ALPp(a), TAM-ALPp(b)-d_1 and TAM-ALPp(c)-d_2 are also shown. (B) Summary of the hyperfine splitting constants for all the structures.

ALP (Tris buffer, pH 7.5, 37 °C, 100 min, Figure 4) was simulated with an 86/14 ratio of the keto TAM-ALPp(b) and the enol TAM-ALPp(a) forms, respectively (see SI Figure S8), showing that even if the species are in equilibrium, it is highly shifted toward the keto form.

Finally, the reaction between TAM-ALPs and ALP was carried out in deuterium oxide (D_2O) to further confirm the molecular structures of the products. The change in EPR spectra between the reaction carried out in H_2O and D_2O (Figure 7A) is in excellent agreement with the isotopic substitution of ^{1}H by ^{2}H of the benzylic protons as expected from the mechanism proposed in Figure 5. Indeed, the spectrum in D_2O can be simulated by replacing the spin of the hydrogen (I = 1/2) with the spin of the deuterium (I = 1) and a decrease of the hyperfine splitting constants by a factor of ~6.5 consistent with their respective gyromagnetic ratios (γ_H = 6.5 γ_D) definitively proving the molecular structures of the TAM-ALPp. Figure 7B shows a summary table of all the resolved hyperfine splitting constants for TAM-ALP substrate and products. To simplify the spectra, other beta-dicarbonyl compounds (acetylacetone and methyl acetoacetate) have also been prepared and characterized; however, all were determined to have stable enol forms under the tested conditions (see SI Figures S4 and S5). Importantly, these molecules provide important information to develop new probes with desired chemical and spectral properties.

In Vitro Imaging of Enzyme Activity Using Overhauser-Enhanced MRI

Next, to demonstrate the feasibility of using TAM-ALPs to image ALP activity, we performed in vitro Overhauser-enhanced MRI measurements of the phantom sample. Figure 8 shows the OMRI images obtained for the TAM-ALPs solutions in the presence and absence of the ALP enzyme. The OMRI images were performed at two frequencies of EPR irradiation; the first one, 460.0 MHz, corresponds to the low-field component of the TAM-ALPs (see Figure 2A), and the second one, 462.5 MHz, corresponds to the low-field component of the product TAM-ALPp(b). The frequency of the low-field component of the TAM-ALPp(b) product was selected to exclude overlap with the components of the substrate and other additional products of the reaction (see

https://doi.org/10.1021/cbmi.4c00059
Chem. Biomed. Imaging 2025, 3, 35−44

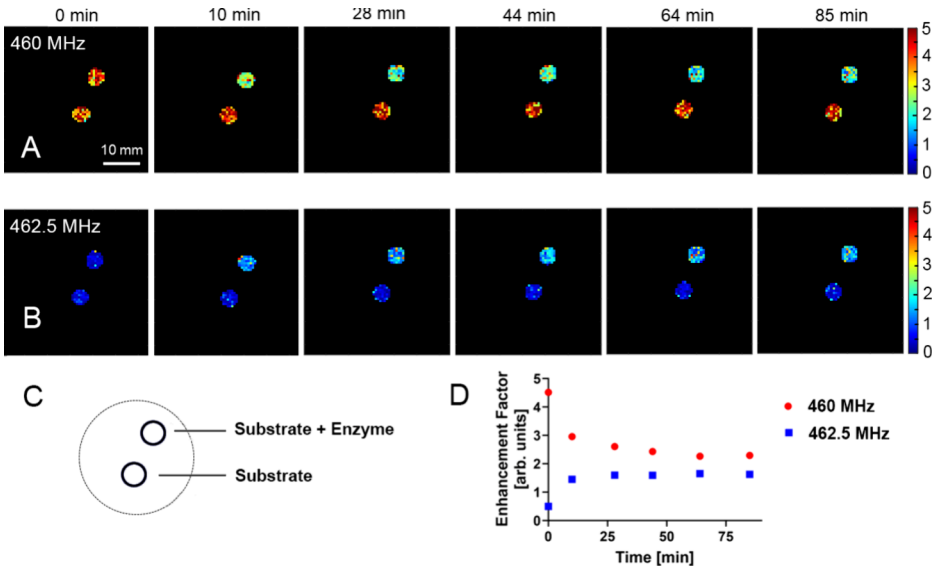

Figure 8. In vitro 2-D OMRI mapping of the ALP activity. (A) Time-evolutions of the MRI enhancement maps were measured at 37 °C at EPR frequencies of the TAM-ALPs substrate; 460.0 MHz, and (B) TAM-ALPp(b) product; 462.5 MHz, for the phantom schematically shown in (C). The phantom consisted of two cylindrical plastic tubes with an inner diameter of 0.5 mm filled with 0.8 mL of solutions of 1.3 mM TAM-ALPs in 10 mM Tris buffer containing 1 mM $MgCl_2$, 0.1 mM $ZnCl_2$, and 0.9% NaCl, pH 7.5. Immediately before scanning, the ALP enzyme (final concentration = 9 U/mL) was added to one of the tubes, as shown on the phantom schematic. (D) Time-course of the averaged enhancement factor for the sample consisting of TAM-ALPs substrate and the enzyme measured at frequency of the substrate and the product. Note that no significant change of the averaged enhancement factor for the sample of the TAM-ALPs substrate in the absence of enzyme was observed. This study demonstrates that the TAM-ALP radical can be used for imaging the enzyme activity.

Figure 5). Note that the collection of a conventional MRI (EPR-off) image is required for the calculation of MRI enhancement. The time-dependences of the enhancement factors of the sample containing ALP enzyme clearly demonstrate a decrease of the enhancements upon irradiation at the substrate frequency of 460 MHz (Figure 8A) and the corresponding increase of the enhancements upon irradiation at the product frequency of 462.5 MHz (Figure 8B), as summarized in Figure 8D. Unfortunately, the presence of several products of the reaction and partial overlap of the EPR spectral lines (see Figure 4) of the substrate and the product, TAM-ALPp(a), complicate further quantitative analysis.

CONCLUSIONS

In conclusion, we have reported the first enzyme-responsive TAM spin probe. The complexity and partial overlap of the EPR spectra of the substrate and enzyme-catalyzed products render the determination of the Michaelis Menten kinetic parameters challenging and are not optional for *in vivo* application. However, we have performed a proof-of-concept imaging of enzyme activity using OMRI. The probe could also be used for EPR imaging in future studies. This work provides essential information for the rational design of a second generation of enzyme-responsive triarylmethyl spin probes with ideal spectral features for *in vivo* imaging applications.

MATERIALS AND METHODS

Synthesis of TAM-ALPs

All solvents were purchased from Fisher Scientific. All commercially available reagents were used as received without further purification. DCM and THF were purified on an Inert Pure Solv Solvent Purification system from Innovative Technologies, Inc. All reactions were carried out under argon in flame-dried glassware and with deoxygenated and anhydrous solvents. Purifications were performed on a Combiflash chromatography system. HRMS spectra were recorded on a Thermofisher Scientific Q Exactive Mass Spectrometer with an electron spray ionization (ESI) source.

Phosphonate Derivative 2. The diester **1** was synthesized according to a known protocol with minor modifications (using 4 eqs of nBuLi and TMEDA).[27] TAM alcohol **1** (400 mg, 0.37 mmol) was dissolved in 200 mL of dry DCM, then triflic acid (66 μL, 0.75 mmol, 2 eqs) was added. The orange solution quickly turned deep blue-green, indicating the conversion of the triarylmethanol to the corresponding cation, and was stirred at room temperature for 2 h. In a second flask, dimethyl acetonylphosphonate (311 μL, 2.25 mmol, 6 eqs) was dissolved in 20 mL of dry THF, then a suspension of sodium hydride (NaH) in mineral oil (90 mg, 60% w/w, 6 eqs) was added at room temperature. There were gases (H_2) released from the solution upon the addition of the hydride, while a white precipitate slowly appeared. The solution was stirred 2 h at room temperature, then cooled down to −78 °C with a dry ice/acetone bath. The solution of TAM cation was transferred dropwise to the phosphonate anion solution at −78 °C, then the flask was removed from the acetone bath and warmed up to room temperature. The reaction mixture was stirred for an hour. The reaction was quenched with 10 mL of 1 M NH_4Cl and extracted with 20 mL of dichloromethane. The organic layer was dried over $MgSO_4$, filtered, and evaporated under reduced pressure. The desired product was purified by flash chromatography, using a gradient from *n*-hexane to ethyl acetate to first elute the radical diester analogue of **1** (**1**$^{\bullet}$), then the desired phosphonate **2** was eluted. After evaporation of the two fractions, 158 mg (35% yield) of the phosphonate **2** was obtained along with 191 mg of the radical diester **1**$^{\bullet}$.

Diphosphorylated Derivative 3. The phosphonate **2** (146 mg, 0.12 mmol) was dissolved in 10 mL of dry THF, then the solution was cooled down to −78 °C using a dry ice/acetone bath. A solution of 1 M freshly prepared LDA (240 μL, 0.24 mmol, 2 eqs) was added, then the reaction mixture was stirred while slowly raising the temperature to −40 °C. Dimethyl chlorophosphate (39 μL, 0.36 mmol, 3 eqs) was added, and the reaction was stirred 10 min at −40 °C then at room temperature for 90 min. The reaction was quenched with 10 mL of 1 M NH_4Cl and extracted with 20 mL of dichloromethane. The organic layer was dried over $MgSO_4$, filtered,

https://doi.org/10.1021/cbmi.4c00059
Chem. Biomed. Imaging 2025, 3, 35−44

and evaporated under reduced pressure. The desired compound was purified by flash chromatography using a gradient from *n*-hexane to ethyl acetate to afford 41 mg of phosphate **3** (26% yield).

TAM-ALPs. TAM **3** (41 mg, 0.03 mmol) was dissolved in 3 mL of dry DCM, and then cooled down with an ice bath. Bromotrimethylsilane (TMSBr) (61 μL, 0.465 mmol, 15 eqs) was added, then the flask was removed from the ice bath, and the reaction mixture was stirred at room temperature for 150 min. The solvent was evaporated, then 2 mL of MeOH was added to the flask and then evaporated. The deprotected phosphate was dissolved in 2 mL methanol and then deoxygenated by bubbling argon for 20 min. An aqueous solution of LiOH 2 M (1 mL) was added then the solution was bubbled with argon for 10 min. The reaction mixture was stirred at 45 °C for 6 h, then acidified to pH = 2 with trifluoroacetic acid. It was purified by reverse-phase chromatography. After washing the column with water containing 0.1% TFA, TAM-ALPs was eluted with 50% acetonitrile in water containing 0.1% TFA. The solution was partially evaporated to remove acetonitrile, then the resulting solution was freeze-dried. The resulting brown powder was resuspended in water and titrated to pH 7 with a solution of NaOH 0.02 M. The now green solution was freeze-dried, affording 34.5 mg of a green powder (83% yield). HRMS calculated for $[C_{42}H_9D_{36}O_{11}P_2S_{12}\bullet]^+$: 1207.1345, found 1207.0073 (see SI Figure S1).

HPLC-MS Analysis

HPLC-MS analyses were carried out using a Water Alliance e2695 separation module, a Water 2998 PDA detector, and a Water SQD2 mass detector. Separations were carried out using a Waters XBridge BEH C18 4.6 mm × 50 mm, 2.5 μm column at 45 °C. Gradient conditions were as follows: Solvent A was water, solvent B acetonitrile, solvent C water containing 1% of trifluoroacetic acid, column temperature: 40 °C; UV detection from 210 to 800 nm, flow rate: 1.5 mL/min. Time 0 min: 80% A, 10% B, 10% C, time 5 min: 0% A, 90% B, 10% C, time 6 min: 100% B.

Electron Paramagnetic Resonance (EPR) Spectroscopy

EPR spectra were recorded using a Bruker ELEXSYS E580 X-band (9.4 GHz) spectrometer. Unless mentioned otherwise, the EPR instrument parameters used were as follows: microwave power: 0.94 mW; sweep width: 10 G; Mod. Amp.: 30 mG; Mod. Freq : 30 kHz, sweep time: 40 s; points: 2048. Solutions were loaded into gas-permeable Teflon tubes with a diameter of 1.14 mm and a wall thickness of 60 μm (Zeus, Inc., USA) and sealed with clay sealant (Kimble Cha-Seal). The temperature and the gas mixture (N_2/O_2) of the samples inside the EPR resonator were controlled using a temperature and gas controller (Noxygen, Germany). EPR spectra were simulated using EasySpin ver. 6.0.2 and MATLAB R2022b.

OMRI Scanner, Pulse Sequence, and Experimental Parameters

The OMRI experiments were performed on an OMRI desktop imager (Keller JXI-KC02, Japan Redox Ltd.) using a standard fast spin echo sequence for MRI. Imaging experiments were performed in 2D modality. The scanning conditions for the OMRI experiment were as follows: repetition time (T_R) × echo time (T_E) × EPR irradiation time (TEP_R), 1000 × 20 × 200 ms; frequencies of EPR irradiation, 460.0 and 462.5 MHz; EPR irradiation power, 8 W; slice thickness, 100 mm, field of view, 40 × 40 mm^2; matrix size, 64 × 64; number of averages, 1; the scanning time of images, was 65 s. Total time of OMRI set 2 EPR frequencies (plus resonator tuning time, approximately 30 s) × 160 s + EPR-off ×65 s = approximately 225 s. MRI detection of 1H water signal was performed on field 0.016 T (0.686 MHz).

Phantom Sample Preparation for OMRI

The phantom consisted of two cylindrical plastic tubes with an inner diameter of 0.5 mm filled with 0.8 mL of solutions of 1.3 mM TAM-ALPs in 10 mM Tris buffer in H_2O containing 1 mM $MgCl_2$, 0.1 mM $ZnCl_2$, and 0.9% NaCl, pH 7.5. The ALP enzyme (final concentration = 9 U/mL) was added to one of the tubes immediately before OMRI acquisition.

■ ASSOCIATED CONTENT

Supporting Information

The Supporting Information is available free of charge at https://pubs.acs.org/doi/10.1021/cbmi.4c00059.

High-resolution mass spectra (HRMS), EPR spectra for pH titration, HPLC-MS data, syntheses and characterization of acetylacetone and methyl acetoacetate TAM radicals, zoom in on spectral features of Figures 2 and 3 (PDF)

■ AUTHOR INFORMATION

Corresponding Author

Benoit Driesschaert − *In Vivo Multifunctional Magnetic Resonance Center, Robert C. Byrd Health Sciences Center, Department of Pharmaceutical Sciences, School of Pharmacy, and C. Eugene Bennett Department of Chemistry, West Virginia University, Morgantown, West Virginia 26506, United States;* orcid.org/0000-0002-1402-413X; Email: Benoit.driesschaert@hsc.wvu.edu

Authors

Murugesan Velayutham − *Department of Biochemistry and Molecular Medicine, School of Medicine and In Vivo Multifunctional Magnetic Resonance Center, Robert C. Byrd Health Sciences Center, West Virginia University, Morgantown, West Virginia 26506, United States;* orcid.org/0009-0001-9751-538X

Martin Poncelet − *In Vivo Multifunctional Magnetic Resonance Center, Robert C. Byrd Health Sciences Center and Department of Pharmaceutical Sciences, School of Pharmacy, West Virginia University, Morgantown, West Virginia 26506, United States*

Ayano Enomoto − *Faculty of Pharmaceutical Sciences, Nagasaki International University, Nagasaki 859-3298, Japan*

Justin L. Huffman − *In Vivo Multifunctional Magnetic Resonance Center, Robert C. Byrd Health Sciences Center and Department of Pharmaceutical Sciences, School of Pharmacy, West Virginia University, Morgantown, West Virginia 26506, United States*

Virat G. Pandya − *In Vivo Multifunctional Magnetic Resonance Center, Robert C. Byrd Health Sciences Center and Department of Pharmaceutical Sciences, School of Pharmacy, West Virginia University, Morgantown, West Virginia 26506, United States*

Kazuhiro Ichikawa − *Faculty of Pharmaceutical Sciences, Nagasaki International University, Nagasaki 859-3298, Japan*

Valery V. Khramtsov − *Department of Biochemistry and Molecular Medicine, School of Medicine and In Vivo Multifunctional Magnetic Resonance Center, Robert C. Byrd Health Sciences Center, West Virginia University, Morgantown, West Virginia 26506, United States;* orcid.org/0000-0001-6187-5546

Complete contact information is available at: https://pubs.acs.org/10.1021/cbmi.4c00059

Notes

The content is solely the responsibility of the authors and does not necessarily represent the official views of the NIH.
The authors declare no competing financial interest.

https://doi.org/10.1021/cbmi.4c00059
Chem. Biomed. Imaging 2025, 3, 35−44

■ ACKNOWLEDGMENTS

This study was partially funded by the National Institute of Health Grant Numbers R21EB028553, R21GM143595, R01EB032321, and R01CA192064.

■ REFERENCES

(1) Hingorani, D. V.; Yoo, B.; Bernstein, A. S.; Pagel, M. D. Detecting Enzyme Activities with Exogenous MRI Contrast Agents. *Chem.—Eur. J.* **2014**, *20* (32), 9840−9850.
(2) Röschmann, P. Radiofrequency penetration and absorption in the human body: Limitations to high-field whole-body nuclear magnetic resonance imaging. *Med. Phys.* **1987**, *14* (6), 922−931.
(3) Swartz, H. M.; Williams, B. B.; Zaki, B. I.; Hartford, A. C.; Jarvis, L. A.; Chen, E. Y.; Comi, R. J.; Ernstoff, M. S.; Hou, H.; Khan, N.; et al. Clinical EPR: Unique Opportunities and Some Challenges. *Acad. Radiol.* **2014**, *21* (2), 197−206.
(4) Enomoto, A.; Ichikawa, K. Research and Development of Preclinical Overhauser-Enhanced Magnetic Resonance Imaging. *Antiox. Red. Sign.* **2022**, *37* (13−15), 1094−1110.
(5) Kishimoto, S.; Krishna, M. C.; Khramtsov, V. V.; Utsumi, H.; Lurie, D. J. In Vivo Application of Proton-Electron Double-Resonance Imaging. *Antiox. Red. Sign.* **2018**, *28* (15), 1345−1364.
(6) Jugniot, N.; Duttagupta, I.; Rivot, A.; Massot, P.; Cardiet, C.; Pizzoccaro, A.; Jean, M.; Vanthuyne, N.; Franconi, J.-M.; Voisin, P.; et al. An elastase activity reporter for Electronic Paramagnetic Resonance (EPR) and Overhauser-enhanced Magnetic Resonance Imaging (OMRI) as a line-shifting nitroxide. *Free Radical Biol. Med.* **2018**, *126*, 101−112.
(7) Audran, G.; Jacoutot, S.; Jugniot, N.; Marque, S. R. A.; Mellet, P. Shifting-Nitroxides to Investigate Enzymatic Hydrolysis of Fatty Acids by Lipases Using Electron Paramagnetic Resonance in Turbid Media. *Anal. Chem.* **2019**, *91* (9), 5504−5507.
(8) Audran, G.; Bosco, L.; Brémond, P.; Franconi, J.-M.; Koonjoo, N.; Marque, S. R. A.; Massot, P.; Mellet, P.; Parzy, E.; Thiaudière, E. Enzymatically Shifting Nitroxides for EPR Spectroscopy and Overhauser-Enhanced Magnetic Resonance Imaging. *Angew. Chem., Int. Ed.* **2015**, *54* (45), 13379−13384.
(9) Sanzhaeva, U.; Xu, X.; Guggilapu, P.; Tseytlin, M.; Khramtsov, V. V.; Driesschaert, B. Imaging of Enzyme Activity by Electron Paramagnetic Resonance: Concept and Experiment Using a Paramagnetic Substrate of Alkaline Phosphatase. *Angew. Chem., Int. Ed.* **2018**, *57* (36), 11701−11705.
(10) Paletta, J. T.; Pink, M.; Foley, B.; Rajca, S.; Rajca, A. Synthesis and Reduction Kinetics of Sterically Shielded Pyrrolidine Nitroxides. *Org. Lett.* **2012**, *14* (20), 5322−5325.
(11) Ovcherenko, S. S.; Raizvich, A. E.; Rogozhnikova, O. Y.; Tormyshev, V. M.; Trukhin, D. V.; Koval, V. V.; Salnikov, G. E.; Genaev, A. M.; Shernyukov, A. V.; Bagryanskaya, E. G. Redox Transformations of the OX063 Radical in Biological Media: Oxidative Decay of Initial Trityl with Further Formation of Structurally-Modified TAM. *Chem.—Eur. J.* **2024**, DOI: 10.1002/chem.202400718.
(12) Ardenkjær-Larsen, J. H.; Laursen, I.; Leunbach, I.; Ehnholm, G.; Wistrand, L. G.; Petersson, J. S.; Golman, K. EPR and DNP Properties of Certain Novel Single Electron Contrast Agents Intended for Oximetric Imaging. *J. Magn. Reson.* **1998**, *133* (1), 1−12.
(13) Epel, B.; Bowman, M. K.; Mailer, C.; Halpern, H. J. Absolute oxygen R1e imaging in vivo with pulse electron paramagnetic resonance. *Magn. Reson. Med.* **2014**, *72* (2), 362−368.
(14) Kishimoto, S.; Devasahayam, N.; Chandramouli, G. V. R.; Murugesan, R.; Otowa, Y.; Yamashita, K.; Yamamoto, K.; Brender, J. R.; Krishna, M. C. Evaluation of a deuterated triarylmethyl spin probe for in vivo R2*-based EPR oximetric imaging with enhanced dynamic range. *Magn. Reson. Med.* **2024**, *91* (1), 413−423.
(15) Gluth, T. D.; Poncelet, M.; DeVience, S.; Gencheva, M.; Hoblitzell, E. H.; Khramtsov, V. V.; Eubank, T. D.; Driesschaert, B. Large-scale synthesis of a monophosphonated tetrathiatriarylmethyl spin probe for concurrent in vivo measurement of pO2, pH and inorganic phosphate by EPR. *RSC Adv.* **2021**, *11* (42), 25951−25954.
(16) Dhimitruka, I.; Bobko, A. A.; Eubank, T. D.; Komarov, D. A.; Khramtsov, V. V. Phosphonated Trityl Probes for Concurrent in Vivo Tissue Oxygen and pH Monitoring Using Electron Paramagnetic Resonance-Based Techniques. *J. Am. Chem. Soc.* **2013**, *135* (15), 5904−5910.
(17) Gluth, T. D.; Poncelet, M.; Gencheva, M.; Hoblitzell, E. H.; Khramtsov, V. V.; Eubank, T. D.; Driesschaert, B. Biocompatible Monophosphonated Trityl Spin Probe, HOPE71, for In Vivo Measurement of pO2, pH, and [Pi] by Electron Paramagnetic Resonance Spectroscopy. *Anal. Chem.* **2022**, *95* (2), 946−954.
(18) Bobko, A. A.; Eubank, T. D.; Driesschaert, B.; Dhimitruka, I.; Evans, J.; Mohammad, R.; Tchekneva, E. E.; Dikov, M. M.; Khramtsov, V. V. Interstitial Inorganic Phosphate as a Tumor Microenvironment Marker for Tumor Progression. *Sci. Rep.* **2017**, *7* (1), 41233.
(19) Eubank, T. D.; Bobko, A. A.; Hoblitzell, E. H.; Gencheva, M.; Driesschaert, B.; Khramtsov, V. V. In Vivo Electron Paramagnetic Resonance Molecular Profiling of Tumor Microenvironment upon Tumor Progression to Malignancy in an Animal Model of Breast Cancer. *Mol. Imaging Biol.* **2024**, *26* (3), 424−434.
(20) Evans, J. V.; Suman, S.; Goruganthu, M. U. L.; Tchekneva, E. E.; Guan, S.; Arasada, R. R.; Antonucci, A.; Piao, L.; Ilgisonis, I.; Bobko, A. A.; et al. Improving combination therapies: targeting A2B-adenosine receptor to modulate metabolic tumor microenvironment and immunosuppression. *J. Natl. Cancer Inst.* **2023**, *115* (11), 1404−1419.
(21) Song, H.; Niu, X.; Ye, K.; Wang, L.; Xu, Y.; Peng, Y. A novel alkaline phosphatase activity sensing strategy combining enhanced peroxidase-mimetic feature of sulfuration-engineered CoOx with electrostatic aggregation. *Anal. Bioanal. Chem.* **2020**, *412* (23), 5551−5561.
(22) Zhao, L.; Xie, S.; Song, X.; Wei, J.; Zhang, Z.; Li, X. Ratiometric fluorescent response of electrospun fibrous strips for real-time sensing of alkaline phosphatase in serum. *Biosens. Bioelectron.* **2017**, *91*, 217−224.
(23) Fawley, J.; Gourlay, D. M. Intestinal alkaline phosphatase: a summary of its role in clinical disease. *J. Surg. Res.* **2016**, *202* (1), 225−234.
(24) Guo, Q.; Miao, M.; Duan, L.; Liu, Y.; Qiu, Y.; Feng, X.; Liang, S.; Xiao, W.; Zheng, M.; Wei, M.; Liu, G. The relationship between insulin resistance, serum alkaline phosphatase, and left ventricular dysfunction following myocardial infarction. *Sci. Rep.* **2023**, *13* (1), 17974.
(25) Kim, T.-H.; Park, S. Y.; Shin, J. H.; Lee, S.; Joo, K. B.; Koo, B. S. Association between changes in serum alkaline phosphatase levels and radiographic progression in ankylosing spondylitis. *Sci. Rep.* **2023**, *13* (1), 9093.
(26) Wang, W.; Li, J.; Liu, Y.; Zhang, W.; Sun, Y.; Ma, P.; Song, D. A Strategy for the Determination of Alkaline Phosphatase Based on the Self-Triggered Degradation of Metal−Organic Frameworks by Phosphate. *Anal. Chem.* **2023**, *95* (6), 3414−3422.
(27) Xia, S.; Villamena, F. A.; Hadad, C. M.; Kuppusamy, P.; Li, Y.; Zhu, H.; Zweier, J. L. Reactivity of Molecular Oxygen with Ethoxycarbonyl Derivatives of Tetrathiatriarylmethyl Radicals. *J. Org. Chem.* **2006**, *71* (19), 7268−7279.
(28) Decroos, C.; Prangé, T.; Mansuy, D.; Boucher, J.-L.; Li, Y. Unprecedented ipso aromatic nucleophilic substitution upon oxidative decarboxylation of tris(p-carboxyltetrathiaaryl)methyl (TAM) radicals: a new access to diversely substituted TAM radicals. *Chem. Commun.* **2011**, *47* (16), 4805−4807.
(29) Rogozhnikova, O. Y.; Vasiliev, V. G.; Troitskaya, T. I.; Trukhin, D. V.; Mikhalina, T. V.; Halpern, H. J.; Tormyshev, V. M. Generation of Trityl Radicals by Nucleophilic Quenching of Tris(2,3,5,6-tetrathiaaryl)methyl Cations and Practical and Convenient Large-Scale Synthesis of Persistent Tris(4-carboxy-2,3,5,6-tetrathiaaryl)-methyl Radical. *Eur. J. Org. Chem.* **2013**, *2013* (16), 3347−3355.

https://doi.org/10.1021/cbmi.4c00059
Chem. Biomed. Imaging 2025, 3, 35−44

(30) Tormyshev, V. M.; Rogozhnikova, O. Y.; Bowman, M. K.; Trukhin, D. V.; Troitskaya, T. I.; Vasiliev, V. G.; Shundrin, L. A.; Halpern, H. J. Preparation of Diversely Substituted Triarylmethyl Radicals by the Quenching of Tris(2,3,5,6-tetrathiaaryl)methyl Cations with C-, N-, P-, and S-Nucleophiles. *Eur. J. Org. Chem.* **2014**, *2014* (2), 371−380.
(31) Sanzhaeva, U.; Poncelet, M.; Tseytlin, O.; Tseytlin, M.; Gencheva, M.; Eubank, T. D.; Khramtsov, V. V.; Driesschaert, B. Synthesis, Characterization, and Application of a Highly Hydrophilic Triarylmethyl Radical for Biomedical EPR. *J. Org. Chem.* **2020**, *85* (16), 10388−10398.
(32) Gao, Y.; Feng, M.; Gao, L.; Leng, Y.; Han, G.; Song, Y.; Liu, Y. Hydroxymethyl-Substituted Tetrathiatriarylmethanol with Variable Reactivity: Selective Access to Three Different Trityl Radicals by Unique Acid-Mediated Reactions. *Eur. J. Org. Chem.* **2024**, *27* (20), No. e202400183.
(33) Tan, X.; Ji, K.; Wang, X.; Yao, R.; Han, G.; Villamena, F. A.; Zweier, J. L.; Song, Y.; Rockenbauer, A.; Liu, Y. Discriminative Detection of Biothiols by Electron Paramagnetic Resonance Spectroscopy using a Methanethiosulfonate Trityl Probe. *Angew. Chem., Int. Ed.* **2020**, *59* (2), 928−934.
(34) Hawkins, M. J.; Powell, E. T.; Leo, G. C.; Gauthier, D. A.; Greco, M. N.; Maryanoff, B. Facile Dephosphonylation of *β*-Ketophosphonic Acids: Mechanistic Studies. *Org. Lett.* **2006**, *8* (16), 3429−3431.
(35) Gust, D.; Mislow, K. Analysis of isomerization in compounds displaying restricted rotation of aryl groups. *J. Am. Chem. Soc.* **1973**, *95* (5), 1535−1547.
(36) Driesschaert, B.; Robiette, R.; Lucaccioni, F.; Gallez, B.; Marchand-Brynaert, J. Chiral properties of tetrathiatriarylmethyl spin probes. *Chem. Commun.* **2011**, *47* (16), 4793−4795.
(37) Driesschaert, B.; Robiette, R.; Le Duff, C. S.; Collard, L.; Robeyns, K.; Gallez, B.; Marchand-Brynaert, J. Configurationally Stable Tris(tetrathioaryl)methyl Molecular Propellers. *Eur. J. Org. Chem.* **2012**, *2012* (33), 6517−6525.
(38) Zhai, W.; Feng, Y.; Liu, H.; Rockenbauer, A.; Mance, D.; Li, S.; Song, Y.; Baldus, M.; Liu, Y. Diastereoisomers of l-proline-linked trityl-nitroxide biradicals: synthesis and effect of chiral configurations on exchange interactions. *Chem. Sci.* **2018**, *9* (19), 4381−4391.

https://doi.org/10.1021/cbmi.4c00059
Chem. Biomed. Imaging 2025, 3, 35−44